Fluorene Derivative Conjugated Polymer Excited State Characterization Through Ultrafast Time Resolved Spectroscopy

Samylla Boazegevski[1], Jeferson Ferreira de Deus[1], Denis Augusto Turchetti[2], Leni Campus Akcelrud[2], Samim Sardar[3], Cosimo D'Andrea[3], Franco Valduga[3], Giulio Cerullo[3], Giovanni Bressan[4], Stephen R Meech[4] and Ismael A. Heisler[5]*

[1] *Departamento de Física, Universidade Tecnológica Federal do Paraná – UTFPR, Av. Sete de Setembro, 3165, Curitiba, Brazil*
[2]*Departamento de Química, Universidade Federal do Paraná, 81531-990 Curitiba, Parana, Brazil*
[3] *IFN-CNR, Dipartimento di Fisica, Piazza Leonardo da Vinci 32, 20133 Milano, Italy*
[4]*School of Chemistry, Norwich Research Park, University of East Anglia, Norwich NR4 7TJ, UK*
[5]*Instituto de Física, Universidade Federal do Rio Grande do Sul - UFRGS, Avenida Bento Gonçalves, 9500, Porto Alegre, Brazil*

Corresponding author ismael.heisler@ufrgs.br

Abstract

A detailed photophysical study of a polymer based on a fluorene derivative is performed through ultrafast nonlinear spectroscopy. The polymer chains are studied in solution, where absorption and emission occur from a disordered distribution of isolated chains, and in solid state as a film, where interchain interactions promote efficient energy transfer. Coherent photoexcitation produces delocalized excitons, which relax and localize on the lowest energy chromophores on the polymer chains on a 100 fs timescale. This is revealed by ultrafast transient absorption spectral evolution, anisotropy relaxation and excited state specific high time resolution fluorescence spectroscopy. The photophysical behavior of the polymer in solution and as a film is significantly different indicating that there is not a significant amount of self-collapsed chain conformations in solution. Compared to solution, in the film, the excited state relaxes an order of magnitude faster, indicating that interchain interactions are strong, promoting efficient energy transfer. The timescales of exciton dynamics revealed in this study will support further theoretical modeling of these polymer structures and are useful for designing blends for use in optoelectronic and electro-optical devices

1. Introduction

Conjugated polymers form a class of materials that have potential applications in various optoelectronic and electro-optical devices. For example, solar cells, organic light-emitting diodes, field effect transistors, sensors, etc.[1–5] These semiconductors have advantages compared to inorganic semiconductors. For instance, the possibility of building devices on flexible substrates, ease of film production over large areas, abundance of available materials and processing at room temperature. The possibility of using simple techniques for deposition of polymeric solutions directly on the substrate is another significant advantage.[6]

Currently, organic semiconductor based device performance and efficiency need to be improved.[7] Apart from the morphology of the films, which is quite critical in the final device performance, a number of other aspects are being studied.[8] Materials that have a high capacity to absorb incident radiation, over a broad spectral range, ideally corresponding to the visible spectral region, are desirable. These absorbed photons produce electron-hole pairs in the active material. The overall efficiency will partly be determined by the dissociation of the electron-hole pairs into free charge carriers and by the mobility of those carriers towards the electrodes, which should be fast and lossless.[7] The photophysical processes in conjugated polymers are quite complex, with a significant amount of questions still open. The elucidation of the nature and mechanisms of the primary steps of exciton dynamics is quite difficult but can have a significant influence on the ensuing photophysical behavior of the material.[9]

In this work, a detailed photophysical study of a polymer based on a fluorene derivative is performed through ultrafast nonlinear spectroscopy. Polyfluorene and its derivatives have been studied since first reported as a blue light-emitting polymer by Yoshino.[10] This group of materials has physical and chemical advantages such as high fluorescence efficiency, good stability and solubility in common organic solvents.[11] Here, the focus will be on one specific fluorene derivative, poly[(9,9-dihexyl-9H-fluorene-2,7-diyl)-1,2-ethenediyl-1,4-phenylene-1,2-ethenediyl], hereafter called LaPPS 16.[12] Recently, this structure has been incorporated in a white light generating blend, aiming applications such as in OLEDs.[13] White light OLEDs are attracting great interest for their possible application as backlight for displays and as lighting sources. A thorough excited state photophysical understanding of LaPPS16 is lacking, and that will be addressed through nonlinear absorption and fluorescence spectroscopy. Specifically the ultrafast, early time relaxation mechanisms will be analyzed and discussed. Such knowledge and understanding of the exciton formation and relaxation on ultrafast timescales might by critical when the material is used in blends for charge separation processes, as it might occur even concomitantly to its operating process.

2. Experiment

LaPPS 16 was synthesized according to reference[12]. A solution of the polymer in toluene was prepared, with optical density (OD) at 412 nm between 0.1 and 0.3, depending on the measurements. A film was prepared with the same solution on a glass substrate, by spin coating.

Transient absorption (TA) spectroscopy was based on a well documented setup and used an amplified Ti:sapphire laser (Libra, Coherent).[14,15] The pulses had a duration around 100 fs at 800 nm and with a repetition rate of 1 KHz. A fraction of the pulse energy was used to pump a homebuilt noncollinear optical parametric amplifier (NOPA) which generates pulses in the visible region. Another fraction of the 800 nm pump pulses is used to generate a white light continuum in a sapphire plate as probe pulses. The measurements were carried out in cuvettes with optical path-length of 1 mm.

Time-Correlated Single Photon Counting (TCSPC) were carried out using a Ti: sapphire laser (Chameleon Ultra II, Coherent, repetition rate of 80 MHz and 140 fs pulse width). A β-barium borate (BBO) crystal was used to frequency double the 720 nm laser output in order to generate the 360 nm excitation wavelength. The fluorescence signal from the sample was focused on the entrance slit of a spectrograph (Acton SP2300i, Princeton Instrument). A streak camera (C5680, Hamamatsu), equipped with the Synchroscan sweep module, which provides spectral-temporal matrices with spectral and temporal resolutions of ∼1 nm and ∼20 ps, respectively, for a temporal window of 2 ns. A CCD (Hamamatsu ORCA-R2 C10600) recorded the streak image. The measurements were carried out in cuvettes with optical path-length of 10 mm.

The femtosecond time resolved fluorescence upconversion setup was already described.[16] Briefly, a Ti:sapphire oscillator produced pulses centred at 800 nm with a pulse duration of 15 fs. The laser output was focussed onto a 50 μm thick Type I BBO crystal with a 150 mm focal length concave mirror to produce up to 5 mW 400 nm second harmonic excitation pump beam. Gate and pump beams were separated with a dichroic mirror. A prism compressor and a pair of chirped mirrors in each arm was used to carefully recompress pump and gate pulses, close to their Fourier transform limit. The pump beam was focused with a 150 mm concave mirror to the centre of a 1 mm pathlength cell which contained the sample. The collection of the fluorescence emitted from the sample and posterior imaging onto the sum-frequency crystal was done with a microscope reflective objective. Finally, fluorescence and gate beams were crossed and focussed onto a 100 μm BBO Type I crystal and the intensity of the upconverted light was detected by a photomultiplier and monochromator combination and measured with a photon counter. The time resolution of the instrument is ~ 50 fs.

3. Results and discussion

A general scheme of the molecular structure of LaPPS 16 is shown in Figure 1a. Normalized steady-state absorption spectra (blue line) and fluorescence spectra (red line) for the polymer dissolved in toluene, are shown in Figure 1b. The low concentration (μM typically) used with a good solvent ensures that the polymer chains are fully solvated and therefore interactions among neighboring chains are not expected. The absorption spectrum is broad (around 100 nm), peaking at 422 nm and mostly featureless, characteristic of polyfluorenes. The fluorescence spectrum is narrower and with characteristic peaks at 481 nm, 508 nm and 550 nm. Those transitions can be associated to vibrations coupled to the electronic transition, also known as vibronic transitions.[17] The energy spacing of around 1300 cm^{-1} indicates that it is a vibronic progression related to C=C stretching vibrations. As Figure 1b shows, the absorption and fluorescence spectra are not mirror images of each other. This indicates that there is some relaxation from the Franck-Condon excited state towards lower energies from where the fluorescence originates.[18]

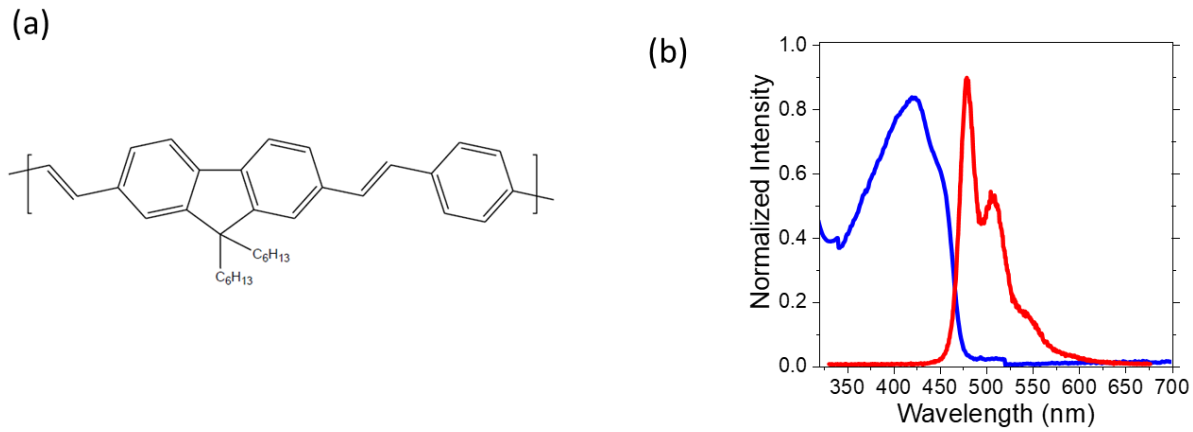

Figure 1. *(a) LaPPS 16 molecular structure. (b) Normalized linear absorption (blue line) and fluorescence spectrum (red line).*

LaPPS 16 is a conjugated polymer with a backbone that has alternating single and double bonds resulting in π-conjugation by π-orbitals overlap. This can lead to significant exciton delocalization along the chain. However due to conformational disorder (as discussed in literature), distortions in the polymer conformation can break up the chain into smaller, so-called chromophores or absorbing subunits.[19,20] Because the excitation energies of these chromophores can present a wide distribution, the polymer absorption spectrum can be broad. In fact, the coupling between the polymer chromophores can lead to electronic excitation being transferred mostly towards the lowest energy chromophores. Assuming the simplest possible description in terms of a particle in a box model, the longest chromophores within the polymer

chain will correspond to the lowest excitation energies. As can be seen in Figure 1b, the distribution of emission energies is narrower when compared to absorption bandwidth. To gain further understanding of the structure and photophysics of LaPPS 16 in solution, nonlinear spectroscopy was applied to the sample.

Figure 2 presents an overview of the transient absorption spectroscopy measurement (given by the transmission change ΔT/T) performed on LaPPS 16 in toluene solution. The pump beam

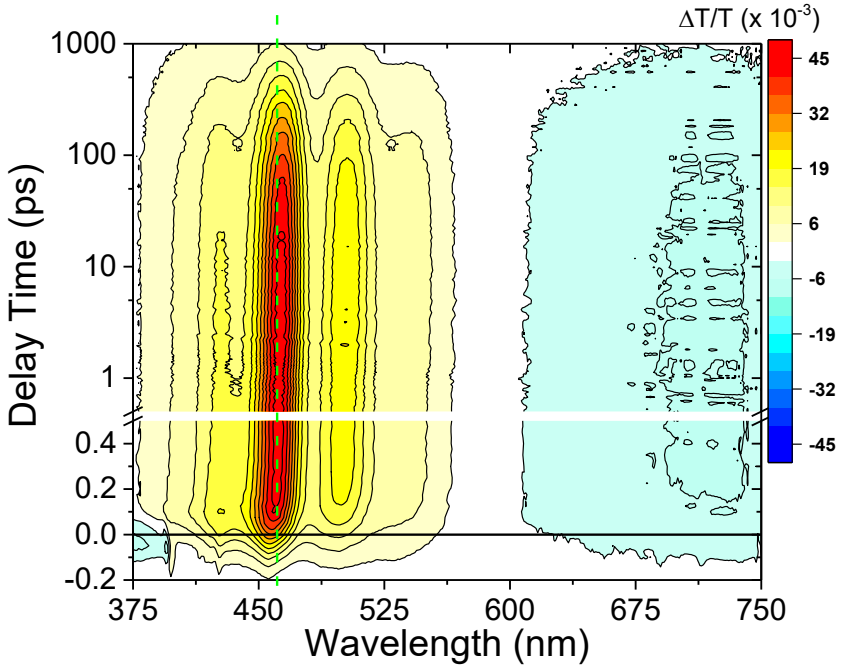

Figure 2. *LaPPS 16 transient absorption spectrum. The amplitude is given by the colour scale.*

was centered at 400 nm and with a typical duration around 100 fs and the relative polarization between pump and probe beams was set at the magic angle (54.7º). The probe beam consisted of a white light spectrum covering a region from 375 nm to 750nm. In Figure 2, the y-axis corresponds to the population delay time. The first picosecond is shown on a linear scale whereas from 1 to 1000 ps the scale is logarithmic. The transmission change, which appears as a color scale ranging from blue to red, is characterized by two distinct regions. From 375 until 550 nm the transmission change is positive, indicating ground state bleach (GSB) and/or stimulated emission (SE). From 600 until 750 nm a negative transmission change indicates a new absorption contribution (ESA) due to transitions from the first excited singlet state up to higher excited states. Apart from intensity changes, a red shift of the signal is visible as highlighted by the green dashed line in Figure 2.

Further analysis of the time resolved data are best performed for specific population delay times, as shown in Figure 3. Noticeable in Figure 3a is that the transmission change has little

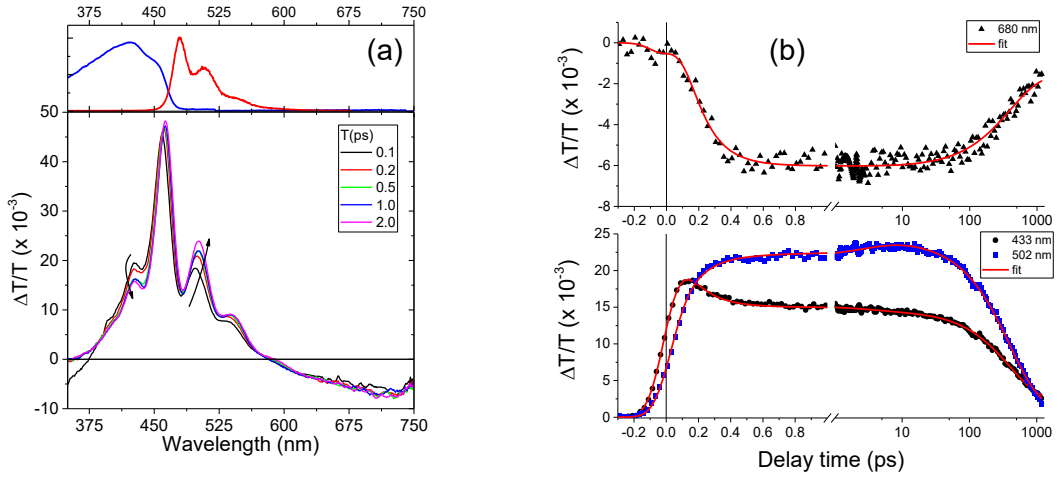

Figure 3. *LaPPS 16 in solution (a) transmission change spectra for population times ranging from 0.1 up to 2 ps. The top graph shows the normalized linear absorption spectrum (blue) and fluorescence spectrum (red). (b) Wavelength specific time resolved curves together with best fit obtained by global fitting analysis.*

amplitude above the pump excitation wavelength of 400 nm. Even at an early delay time of 100 fs, the transient spectrum has a significantly different shape from what would be expected from the linear absorption spectrum.[21] This is an indication that the ground state population is inhomogeneously broadened, in line with the conformational disorder discussed above.[20] Another evident feature is that at early delay times, there is a fast dynamical evolution resulting in an amplitude decrease of the GSB/SE, as indicated by a downward arrow around 430 nm in Figure 3a. Concomitantly the peaks at 480, 509 and 550 nm increase in amplitude as well as red shift. This is indicated in Figure 3a by an upward arrow. Furthermore, although not so noticeable, the negative transmission change above 600 nm becomes more negative during this fast early time population evolution. These dynamics are better captured by observing the transmission change as a function of time for specific probe wavelengths, as shown in Figure 3b. Three specific wavelengths were chosen, corresponding to dynamics within GSB (433 nm), SE (502 nm) and ESA (680 nm). One can observe a complete correspondence of the evolution of the transmission change amplitude for these three wavelengths at early and long delay times.

In order to rule out fast dynamics due to multiple exciton formation in the absorbing units by excessive pump energy, a set of pump energy dependence measurements were performed. For high pump energies, there is a probability that more than one exciton can be generated on the same polymer chain.[22] When multiple excitons are in close spatial proximity they might annihilate, promoting fast GSB recovery and excited state population decay. Figure S1 shows time resolved transmission change at 426 nm for four different pump energies. As expected in Figure S1a, the amplitude of the transmission change increases with pump energy but no

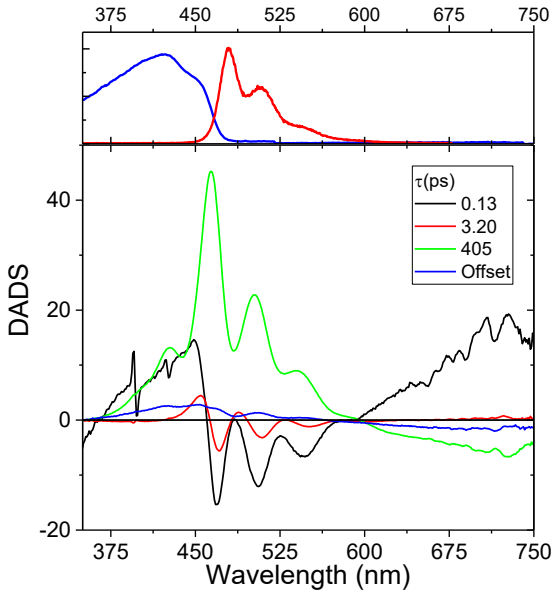

Figure 4. *Decay-associated difference spectra (DADS). The top graph shows the normalized linear absorption spectrum (blue) and fluorescence spectrum (red).*

additional, fast relaxation is noticeable. In Figure S1b the data are plotted on a linear-log scale, where the curves were multiplied by a factor so that all matched the lowest energy curve for population delay times above 1 ps. As can be seen, only for the highest pump energy a small extra relaxation during the first picosecond might be present. Therefore, the pump energy was kept at 8.5 nJ.

In order to determine the relaxation timescales present in the measured data, a global fitting analysis, using Glotaran, was applied to the full transient absorption measurement.[23] As no *a priori* knowledge about the detailed kinetic model for data is known, the simplest possible scheme capable of capturing the dynamical evolution was utilized. This consists of a parallel decay scheme convoluted with the instrument response function and a factor correcting for probe beam temporal dispersion.[24] The lineshapes obtained using this model are shown in Figure 4 and are termed decay-associated difference spectra (DADS). These lineshapes are plots of the resulting pre-exponential factors obtained after globally fitting the datasets to a linear sum of exponentials. A negative (positive) DADS in a region were the measured signal has negative (positive) amplitude translates into a decaying (rising) exponential contribution. For positive measured signals, the assignment is exactly the opposite, i.e., a negative (positive) DADS translates into rising (decaying) exponential contributions. The best fit was obtained with a minimum of three exponential terms plus a constant offset. Examples of the resulting fit can be seen as the red curves going through the data shown in Figure 3b. The fastest exponential was fit with a time constant of 130 fs. The corresponding DADS (black curve in Figure 4) shows a positive amplitude in the GSB spectral region (below ~450 nm) and therefore accounts

for a fast ground state recovery and/or SE decay. The negative peaks at 480, 502 and 550 nm account for the risetime observed in the SE amplitude. A positive contribution of this DADS for wavelengths above 600 nm accounts for a risetime in the ESA signal. The second exponential was fit with a time constant of 3.20 ps. As can be seen in Figure 4 (red curve), this DADS has an overall small amplitude, and contributes (mostly) negatively in the region of the SE and positively in the ESA. Therefore, it accounts for a slower contribution to the risetime of the SE and ESA signals. The last exponential term was fit with a time constant of 405 ps and its DADS (green curve in Figure 4) makes the highest contribution to the overall amplitude. As this DADS is positive in the GSB and SE regions and negative in the ESA region, it accounts for the simultaneous decay of those signals back to the ground state. Therefore, it can be interpreted as the full re-equilibration of the ground state population. This is confirmed by measuring the fluorescence decay through TCSPC (Time-Correlated Single-Photon Counting) as shown in Figure S2a. The integrated fluorescence decays with a time constant of 450 ps, which is in agreement with the recovered 405 ps decay time in the TA measurement.

Another important observable is given by anisotropy, as shown in Figure 5, which was obtained by averaging the over the SE spectral region. Even at the shortest delay times, the anisotropy is smaller than 0.4 (~0.35). There is a fast initial evolution followed by slower

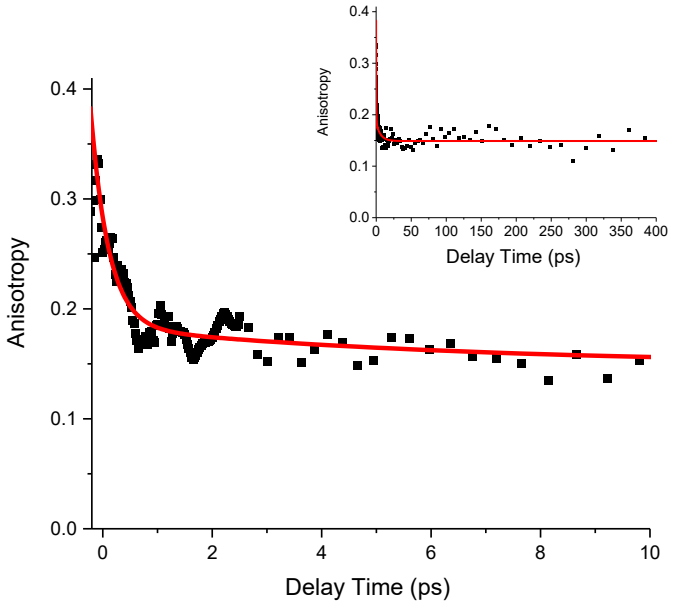

Figure 5*. LaPPS 16 anisotropy obtained by averaging the over the SE spectral region. The inset shows full scale anisotropy.*

dynamics. The inset in Figure 5 shows the full evolution, over 400 ps, which is the typical excited state lifetime. After the initial fast evolution, the anisotropy remains constant with a value of ~0.15. The data were fit with two exponentials and a constant offset. The time constants were fixed to the already retrieved population relaxation time constants, 130 fs and

3.2 ps. As can be seen in Figure 5, the fitting is excellent, confirming that the anisotropy does indeed relax on the same timescale as the population relaxation.

The TA data presented so far indicates the exciton population is moving towards lower energy, as revealed by emission red-shifting and ESA amplitude increase, on a fast timescale whose exact determination might be limited by experiment time resolution of ~100 fs. Furthermore this is matched by anisotropy relaxation on the same timescale. To be able to investigate in more detail the fast relaxation observed in the TA measurements, excited state specific information was obtained by time resolved fluorescence spectroscopy. This method selectively probes neutral singlet excitations and therefore is not sensitive to any other nonradiative relaxation mechanisms, including formation of charged polarons or triplet states. This contrasts and complements the TA data already presented.

Figure 6a shows two specific emission wavelengths whereas Figure S3 presents the full set of emission wavelengths that where measured. The curves where multiplied by a factor such that their decay amplitude matches after 10 ps. One can observe a fast decay on the blue side of the fluorescence spectrum (452nm) and a concomitant risetime on the red side (547 nm). The data were globally fit with three exponential terms. The resulting pre-exponential amplitudes are shown in figure 6b. The fastest exponential decays with a time constant of 50 fs, followed by a weak contribution with an exponential decay time constant of 5.2 ps. The longest exponential decays with a time constant of 494 ps, which matches well the longest contribution retrieved by TA measurements and by TCSPC, already reported above. Therefore, one can assign this to the full relaxation of the singlet exciton population back to the ground state. The fastest decay constant is within the time resolution of the instrument (~ 50 fs). As it has a positive amplitude on the blue edge of the fluorescence spectrum (decay) and a negative amplitude on the red side (risetime) it must be related to a spectral shift towards lower energies of the excited state population. There is good correspondence between this fast fluorescence amplitude relaxation with the fastest recovered TA DADS, as shown in Figure S4. This indicates that the longer time constant revealed by the TA DADS (130 fs) is in fact limited by the instrument response function, which in that case was (~ 100 fs). Furthermore, it suggests that the fastest DADS in TA has no GSB recovery contribution but is solely given by exciton relaxation within the excited state.

The fastest components recovered by TA and time resolved fluorescence measurements are too fast to be assigned to energy transfer mechanisms such as Förster resonance energy transfer (FRET).[25,26] As discussed in literature, self-localization of the photogenerated exciton into a smaller number of repeat units occurs typically within 100 fs.[27] Following previous

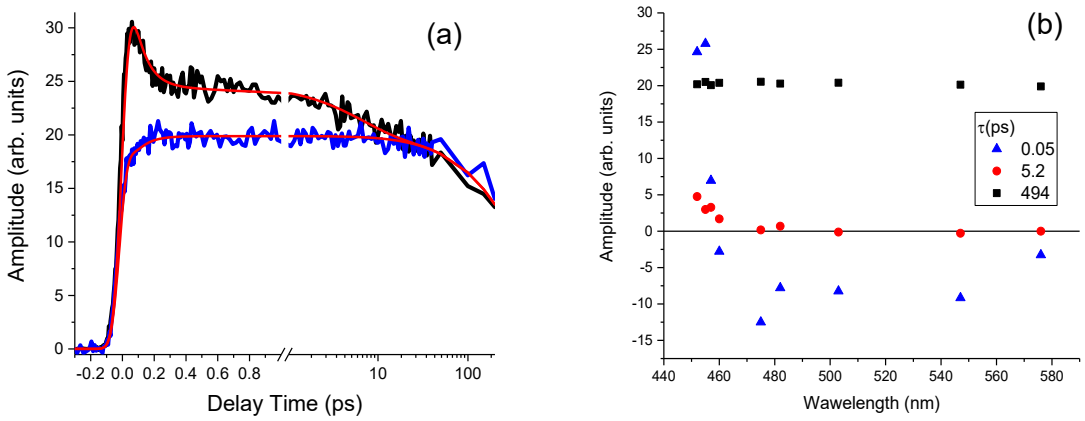

Figure 6. *Time resolved fluorescence measurements. (a) Curves at emission wavelengths 452 nm (black) and 547 (nm) blue and fit (red). (b) Pre-exponential factors as a function of wavelengths obtained by fitting globally all the emission wavelengths.*

assignments, we attribute the population and anisotropy dynamics to a combination of processes that relax these observables very rapidly, within the pulse overlap timescale in our experiment.[25,28] The ultrafast photoexcitation produces an exciton that will be initially delocalized over a significant portion of the polymer chain. However due to coupling to the bath of nuclear motions, as reflected by the vibronic progression discussed above, rapid exciton relaxation and localization will occur.[20] Although there is no significant movement along the chain, the spatial exciton wavefunction contraction and localization can rotate the transition dipole moment and therefore change anisotropy. After fast exciton localization, further anisotropy relaxation can occur through electronic excitation transfer to nearby absorbing units in the polymer, typically within a radius of ~10 nm by FRET. Although a decaying component with a time constant of 3.2 ps was observed in TA and around 5.2 ps in time resolved fluorescence, it is weak in both measurements. This observation, of a weak picosecond contribution, indicates that there is not a significant amount of self-collapsed chain conformations. If it where the case, then the distance between segments would be short enough so that excitation energy could be efficiently funneled, through FRET, towards the lowest energy conjugated segments. This because a significant number of segments would be effectively within the Förster radius. And that is indeed what happens when LaPPS 16 is prepared as a film.

The TA spectroscopy results for the film are shown in Figure 7a, for delay times ranging from 0.1 to 10 ps, and Figure S5 for the time resolved fluorescence, which compares relaxation at two emission wavelengths for LaPPS 16 in solution and film. A striking difference between the measurements performed in solution when compared to the film is the much faster overall

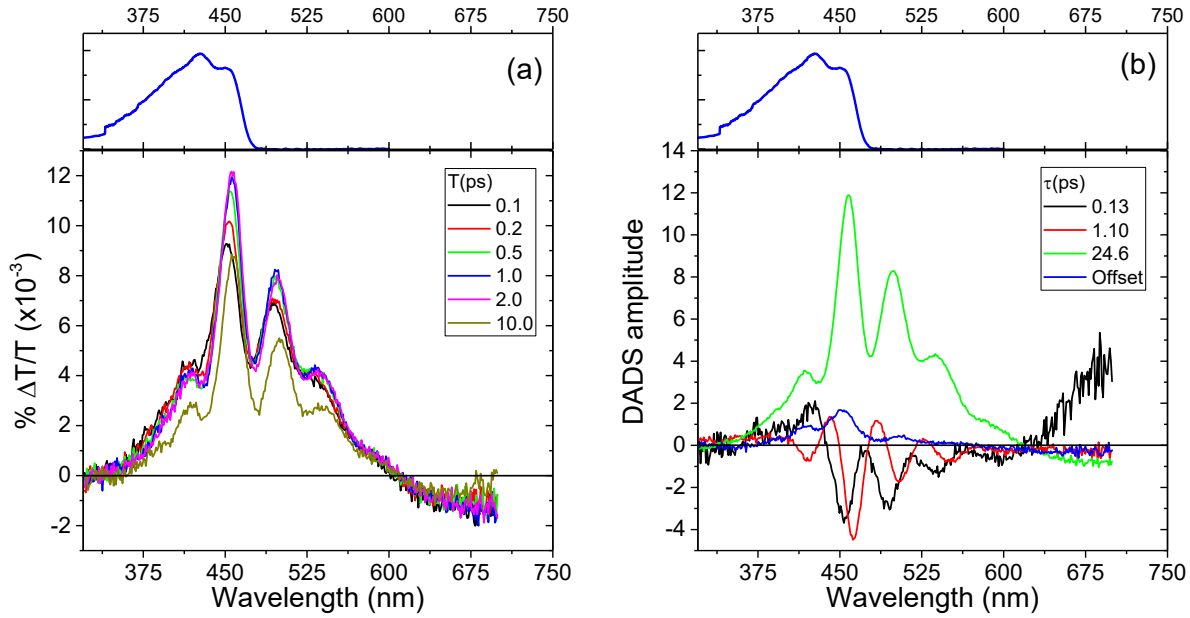

Figure 7 *LaPPS 16 film (a) transmission change spectra for population times ranging from 0.1 up to 10 ps. The top graph shows the normalized linear absorption spectrum (blue). (b) Decay-associated difference spectra (DADS).*

relaxation in the latter.[29] This is highlighted in Figure S6 where the amplitude at one specific wavelength (428 nm – GSB region) is compared. Care was taken to avoid dynamics due to multiple exciton formation, by working with pulses with low enough energy (see Figure S1 (c)). The GSB recovers at least one order of magnitude faster in the film when compared to the polymer in solution. A global analysis of the film requires three exponential terms with time constants of 0.13 and 1.10 ps and 24.6 ps, plus an offset accounting for long lived species (most likely triplet state population). The recovered DADS are shown in Figure 7b. Observing the shapes of these DADS curves and comparing them to the recovered DADS curves for LaPPS 16 in solution, it is possible to notice great similarity between them, apart from differences in the relative amplitudes. Given that the fastest component could be fit with the same time constant of 130 fs, it is assigned to the same dynamics for the sample either in film or solution. However, the other two recovered time constants are shorter for the film. This alteration must be related to the fact that in the films the chains are in close proximity and in contact to each other. This approximation can lead to interchain FRET. Therefore, the DADS with a time constant of 1.1 ps, as for the case when the sample is in solution, can be assigned to FRET that is accelerated in the film. As reported in the literature, interchain FRET is generally faster than intrachain energy transfer for a number of polymeric structures. Anisotropy decay further supports this assignment. Figure S7 compares the measured anisotropy for the film with the one measured for the sample in solution. In both cases the anisotropy shows a fast initial

relaxation. However, for the film, the anisotropy continues to relax and reaches a value around zero, meaning a complete transition dipole moment randomization, within 10 ps. This contrasts with the solution, where after the initial fast relaxation, a weak 3 ps relaxation leads the anisotropy to remain constant after 10 ps. The implication is that in the film, due to close proximity of the polymer chains, efficient interchain energy transfer can occur through FRET, which randomizes the transition dipole moment and, therefore, decreases the anisotropy value.

The most striking difference between film and solution is the longest component, which for LaPPS 16 in solution decays with a time constant of 405 ps, whereas for the film decays with a much faster 24.6 ps time constant, i.e., a signification acceleration. The fact that the GSB recovers much faster in the film when compared to solution indicates that the approximation of the chains introduces a new nonradiative ground state re-equilibration channel. The exact mechanism responsible for this nonradiative relaxation is difficult to determine without further theoretical modeling, but has been observed before for other polymeric structures.

In summary, photoexcitation of LaPPS 16 produces electrons and holes considerably delocalized along the polymer chain.[26] The interaction of this quantum coherent excitation with the environment provided by the polymer chain vibrations, rotations and solvent molecules produces decoherence and, therefore, as a function of time, the superposition of states will lose its coherence. Since those interactions are localized on specific regions of the polymer, a spatial loss of coherence will also follow.[30] The correlations between spatially distant parts of the photoexcitation on the polymer will be lost and the equilibrium states can become localized. Our results indicate that for LaPPS 16 in solution the exciton relaxes to its lowest energy state mostly through a fast coherent process, and not by incoherent hopping among chromophores.[31] FRET becomes important for LaPPS 16 when cast as a film, when interchain energy transfer becomes very efficient. Given the high time resolution of the time-resolved fluorescence up-conversion method, detailed information about the early time relaxation dynamics of photoexcited singlet state population could be retrieved. The sub 100 fs amplitude shift towards lower energy, indicating an ultrafast energy lowering mechanism for the excitons in LaPPS 16. The most likely mechanism, based on experimental and theoretical results, points to a coherent localization of the exciton on lower energy emitting subunits in the polymer chains. An understanding of the ultrafast early time relaxation mechanisms might be critical for a full understanding of charge separation processes in blends as it might occur concomitantly.

4. Conclusions

Detailed insights into the excited state photophysics for LaPPS 16 were obtained by ultrafast nonlinear spectroscopy, followed by global analysis of the transient absorption and fluorescence time curves. The linear absorption spectrum is inhomogeneously broadened, due to ground state conformational disorder.[32–34] However, TA data revealed a weak picosecond relaxation contribution, indicating that there is not a significant amount of self-collapsed chain conformations. The chains are well solvated and separated in solution, so disorder comes from small angle rotations around bonds along the backbone of the conjugated chains and therefore it is broken into conformational subunits, which are the absorbing chromophores.[25]

A fast relaxation component observed in TA and time resolved fluorescence revealed that the delocalized photoexcitation along the polymer chain localizes the exciton and the overall conjugated polymer energy very efficiently. In solution, this is the main exciton relaxation mechanism, as only a weak picosecond relaxation component was observed and which could be ascribed to FRET energy transfer. However when cast as a film, FRET becomes efficient, funneling energy and opening a nonradiative route to excited state relaxation. The excited population relaxes an order of magnitude faster compared to the case where the polymer is in solution. This information has to be taken into account when planning to use this polymer as a donor, in which case it might be ineffective in a film, as most energy might be lost before charge separation can occur.[35]

As shown in this work, corroborating ongoing discussions in literature, conjugated polymers have a complex photophysical response, above all during the very early times after photoexcitation.[25] This creates significant difficultly in providing detailed descriptions and assigning specific relaxation mechanisms during this period. As has been pointed out, on different levels, multiple competing processes might be contributing, including exciton localization followed by delocalization and self-trapping. Furthermore, other relaxation mechanisms might be at play, including energy minimization within the exciton manifold, or polaron formation and recombination. Differently from inorganic semiconductors, where a general theory describes their behavior quite well, organic semiconductors are much more complex and specific descriptions have to be developed, connected to the specific molecular structures upon which the material rely.

Acknowledgements

We would like to thank Prof. Steve Meech, for hosting IAH and providing access to the time resolved up conversion fluorescence spectroscopy setup. We would like to thank Prof. Giulio Cerullo for providing accommodation for SB and laboratory access for the TA measurements. We would like to thank Prof. Cosimo D'Andrea for access to streak camera setup access and Mr. Samim Sardar for helping to perform picosecond time-resolved fluorescence measurements. We would like to thank the DAFIS department of UTFPR for providing funding for SB, including flight tickets.

References

(1) Gnida, P.; Amin, M. F.; Pajak, A. K.; Jarzabek, B. Polymers in High-Efficiency Solar Cells: The Latest Reports. *Polymers (Basel).* **2022**, *14* (10). https://doi.org/10.3390/polym14101946.

(2) Matindoust, S.; Farzi, G.; Nejad, M. B.; Shahrokhabadi, M. H. Polymer-Based Gas Sensors to Detect Meat Spoilage: A Review. *React. Funct. Polym.* **2021**, *165* (December 2020), 104962. https://doi.org/10.1016/j.reactfunctpolym.2021.104962.

(3) Li, M.; Wang, J.; Xu, W.; Li, L.; Pisula, W.; Janssen, R. A. J.; Liu, M. Noncovalent Semiconducting Polymer Monolayers for High-Performance Field-Effect Transistors. *Prog. Polym. Sci.* **2021**, *117*, 101394. https://doi.org/10.1016/j.progpolymsci.2021.101394.

(4) Borges, B. G. A. L.; Gioti, M.; Correa, R. S.; Andreopoulou, A. K.; Veiga, A. G.; Laskarakis, A.; Kallitsis, J. K.; Logothetidis, S.; Rocco, M. L. M. Surface, Interface and Electronic Studies on Anthracene Derived Polymeric Thin Films for OLED Applications. *Opt. Mater. (Amst).* **2021**, *117* (April 2020), 111145. https://doi.org/10.1016/j.optmat.2021.111145.

(5) Jin, L.; Ma, R.; Liu, H.; Xu, W.; Luo, Z.; Liu, T.; Su, W.; Li, Y.; Lu, R.; Lu, X.; Yan, H.; Tang, B. Z.; Yang, T. Boosting Highly Efficient Hydrocarbon Solvent-Processed All-Polymer-Based Organic Solar Cells by Modulating Thin-Film Morphology. *ACS Appl. Mater. Interfaces* **2021**, *13* (29), 34301–34307. https://doi.org/10.1021/acsami.1c07946.

(6) Catania, F.; De Souza Oliveira, H.; Lugoda, P.; Cantarella, G.; Münzenrieder, N. Thin-Film Electronics on Active Substrates: Review of Materials, Technologies and Applications. *J. Phys. D. Appl. Phys.* **2022**, *55* (32). https://doi.org/10.1088/1361-6463/ac6af4.

(7) Wang, J.; Wen, S.; Hu, J.; Han, J.; Yang, C.; Li, J.; Bao, X.; Yan, S. High-Efficiency Ternary Sequential Solution Deposition Structure Organic Solar Cells with Two Polymer Donors. *Chem. Eng. J.* **2023**, *452* (P4), 139462. https://doi.org/10.1016/j.cej.2022.139462.

(8) Dimitriev, O. P. Dynamics of Excitons in Conjugated Molecules and Organic Semiconductor Systems. *Chem. Rev.* **2022**, *122* (9), 8487–8593. https://doi.org/10.1021/acs.chemrev.1c00648.

(9) Dimitriev, O. P. Dynamics of Excitons in Conjugated Molecules and Organic Semiconductor Systems. *Chemical Reviews*. American Chemical Society 2021.

https://doi.org/10.1021/acs.chemrev.1c00648.

(10) Fukuda, M.; Sawada, K.; Yoshino, K. Synthesis of Fusible and Soluble Conducting Polyfluorene Derivatives and Their Characteristics. *J. Polym. Sci. Part A Polym. Chem.* **1993**, *31* (10), 2465–2471. https://doi.org/10.1002/pola.1993.080311006.

(11) Xie, L.-H.; Yang, S.-H.; Lin, J.-Y.; Yi, M.-D.; Huang, W. Fluorene-Based Macromolecular Nanostructures and Nanomaterials for Organic (Opto)Electronics. *Philos. Trans. R. Soc. A Math. Phys. Eng. Sci.* **2013**, *371* (2000), 20120337. https://doi.org/10.1098/rsta.2012.0337.

(12) Nowacki, B.; Iamazaki, E.; Cirpan, A.; Karasz, F.; Atvars, T. D. Z.; Akcelrud, L. Highly Efficient Polymer Blends from a Polyfluorene Derivative and PVK for LEDs. *Polymer (Guildf).* **2009**, *50* (25), 6057–6064. https://doi.org/10.1016/j.polymer.2009.09.056.

(13) Franchello, F.; de Menezes, L. C. W.; Renzi, W.; Laureto, E.; Turchetti, D. A.; Akcelrud, L. C.; de Deus, J. F.; Duarte, J. L. Achieving White Emission from Solution Processable Blends of Polyvinylene Derivative Guests into a Polyfluorene Matrix. *J. Electron. Mater.* **2019**, *48* (9), 5980–5987. https://doi.org/10.1007/s11664-019-07350-z.

(14) Cerullo, G.; Manzoni, C.; Lüer, L.; Polli, D. Time-Resolved Methods in Biophysics. 4. Bbroadband Pump–Probe Spectroscopy System with Sub-20 Fs Temporal Resolution for the Study of Energy Transfer Processes in Photosynthesis. *Photochem. Photobiol. Sci.* **2007**, *6* (2), 135–144. https://doi.org/10.1039/b606949e.

(15) Polli, D.; Lüer, L.; Cerullo, G. High-Time-Resolution Pump-Probe System with Broadband Detection for the Study of Time-Domain Vibrational Dynamics. *Rev. Sci. Instrum.* **2007**, *78* (10). https://doi.org/10.1063/1.2800778.

(16) Heisler, I. A.; Kondo, M.; Meech, S. R.; Heisler, I. A.; Kondo, M.; Meech, S. R. Reactive Dynamics in Confined Liquids : Ultrafast Torsional Dynamics of Auramine O in Nanoconfined Water in Aerosol OT Reverse Micelles Reactive Dynamics in Confined Liquids : Ultrafast Torsional Dynamics of Auramine O in Nanoconfined Water in Aerosol OT . **2009**. https://doi.org/10.1021/jp808989f.

(17) Stevens, M. A.; Silva, C.; Russell, D. M.; Friend, R. H. Exciton Dissociation Mechanisms in the Polymeric Semiconductors Poly(9,9-Dioctylfluorene) and Poly(9,9-Dioctylfluorene-Co-Benzothiadiazole). *Phys. Rev. B - Condens. Matter Mater. Phys.* **2001**, *63* (16). https://doi.org/10.1103/PhysRevB.63.165213.

(18) Park, K. H.; Kim, W.; Yang, J.; Kim, D. Excited-State Structural Relaxation and

Exciton Delocalization Dynamics in Linear and Cyclic π-Conjugated Oligothiophenes. *Chem. Soc. Rev.* **2018**, *47* (12), 4279–4294. https://doi.org/10.1039/c7cs00605e.

(19) Hwang, I.; Scholes, G. D. Electronic Energy Transfer and Quantum-Coherence in π-Conjugated Polymers. *Chem. Mater.* **2011**, *23* (3), 610–620. https://doi.org/10.1021/cm102360x.

(20) Dykstra, T. E.; Hennebicq, E.; Beljonne, D.; Gierschner, J.; Claudio, G.; Bittner, E. R.; Knoester, J.; Scholes, G. D. *Conformational Disorder and Ultrafast Exciton Relaxation Dynamics in PPV-Family Conjugated Polymers*.

(21) Berera, R.; van Grondelle, R.; Kennis, J. T. M. Ultrafast Transient Absorption Spectroscopy: Principles and Application to Photosynthetic Systems. *Photosynthesis Research*. September 2009, pp 105–118. https://doi.org/10.1007/s11120-009-9454-y.

(22) Bressan, G.; Jirasek, M.; Anderson, H. L.; Heisler, I. A.; Meech, S. R.; Meech, S. R. Exciton-Exciton Annihilation as a Probe of Exciton Diffusion in Large Porphyrin Nanorings. *J. Phys. Chem. C* **2020**, *124* (34), 18416–18425. https://doi.org/10.1021/acs.jpcc.0c04546.

(23) Snellenburg, J. J.; Laptenok, S.; Seger, R.; Mullen, K. M.; van Stokkum, I. H. M. Glotaran: A Java-Based Graphical User Interface for the R Package TIMP. *J. Stat. Softw.* **2012**, *49* (3), 1–22. https://doi.org/10.18637/jss.v049.i03.

(24) Van Stokkum, I. H. M.; Larsen, D. S.; Van Grondelle, R. Global and Target Analysis of Time-Resolved Spectra. *Biochimica et Biophysica Acta - Bioenergetics*. Elsevier July 9, 2004, pp 82–104. https://doi.org/10.1016/j.bbabio.2004.04.011.

(25) Hwang, I.; Scholes, G. D. Electronic Energy Transfer and Quantum-Coherence in π-Conjugated Polymers. *Chem. Mater.* **2011**, *23* (3), 610–620. https://doi.org/10.1021/cm102360x.

(26) Barford, W. Exciton Dynamics in Conjugated Polymer Systems. *Front. Phys.* **2022**, *10* (October), 1–22. https://doi.org/10.3389/fphy.2022.1004042.

(27) Ruseckas, A.; Wood, P.; Samuel, I. D. W.; Webster, G. R.; Mitchell, W. J.; Burn, P. L.; Sundström, V. Ultrafast Depolarization of the Fluorescence in a Conjugated Polymer. *Phys. Rev. B - Condens. Matter Mater. Phys.* **2005**, *72* (11), 1–5. https://doi.org/10.1103/PhysRevB.72.115214.

(28) Gonzalvez Perez, I.; Barford, W. Ultrafast Fluorescence Depolarization in Conjugated Polymers. *J. Phys. Chem. Lett.* **2021**, *12* (22), 5344–5348. https://doi.org/10.1021/acs.jpclett.1c01354.

(29) Peckus, D.; Devižis, A.; Hertel, D.; Meerholz, K.; Gulbinas, V. Exciton Diffusion,

Annihilation and Their Role in the Charge Carrier Generation in Fluorene Based Copolymers. *Chem. Phys.* **2012**, *404*, 42–47. https://doi.org/10.1016/j.chemphys.2012.02.003.

(30) Barford, W.; Mannouch, J. R. Torsionally Induced Exciton Localization and Decoherence in π -Conjugated Polymers. *J. Chem. Phys.* **2018**, *149* (21). https://doi.org/10.1063/1.5054176.

(31) Grage, M. M.-L.; Zaushitsyn, Y.; Yartsev, A.; Chachisvilis, M.; Sundström, V.; Pullerits, T. Ultrafast Excitation Transfer and Trapping in a Thin Polymer Film. *Phys. Rev. B* **2003**, *67* (20), 205207. https://doi.org/10.1103/PhysRevB.67.205207.

(32) Volpato, A.; Zerbetto, M.; Bolzonello, L.; Meneghin, E.; Fresch, B.; Benelli, T.; Giorgini, L.; Collini, E. Effect of Different Conformational Distributions on the Ultrafast Coherence Dynamics in Porphyrin-Based Polymers. *J. Phys. Chem. C* **2019**, *123* (16), 10212–10224. https://doi.org/10.1021/acs.jpcc.8b12562.

(33) Makhov, D. V.; Barford, W. Local Exciton Ground States in Disordered Polymers. *Phys. Rev. B - Condens. Matter Mater. Phys.* **2010**, *81* (16), 1–6. https://doi.org/10.1103/PhysRevB.81.165201.

(34) Singh, J.; Bittner, E. R.; Beljonne, D.; Scholes, G. D. Fluorescence Depolarization in Poly[2-Methoxy-5-((2-Ethylhexyl)Oxy)-1,4- Phenylenevinylene]: Sites versus Eigenstates Hopping. *J. Chem. Phys.* **2009**, *131* (19). https://doi.org/10.1063/1.3259549.

(35) Proctor, C. M.; Kuik, M.; Nguyen, T. Q. Charge Carrier Recombination in Organic Solar Cells. *Prog. Polym. Sci.* **2013**, *38* (12), 1941–1960. https://doi.org/10.1016/j.progpolymsci.2013.08.008.